Projectile velocity dependence of emission line polarization degrees following slow Ar^{8+}-Li($2s$) state-selective electron-capture collisions

C. Laulhé,[1] E. Jacquet,[1,2] G. Cremer,[1,2] J. Pascale,[3] Ph. Boduch,[1,2] G. Rieger,[1,2] M. Chantepie,[1,2] and D. Lecler[1]
[1]*Laboratoire de Spectroscopie Atomique, CNRS-ERS 137, ISMRA, Boulevard Maréchal Juin, 14050 Caen Cedex, France*
[2]*UFR des Sciences, Université de Caen, Esplanade de la Paix, 14032 Caen Cedex, France*
[3]*Service des Photons, Atomes et Molécules, CEA, Centre d'Etudes de Saclay, Bâtiment 522, 91191 Gif sur Yvette Cedex, France*
(Received 30 May 1996)

The influence of the projectile velocity on the m_ℓ distributions of the Ar^{7+} excited states produced by electron capture during Ar^{8+}-Li($2s$) collisions is studied experimentally between 1.5 and 4.5 keV amu^{-1} by measuring the polarization of the emitted light, and theoretically between 1 and 4 keV amu^{-1} by using the classical trajectory Monte Carlo (CTMC) method. We investigate the $7\ell'$-8ℓ and $8\ell'$-9ℓ radiative transitions subsequent to the decay of the 8ℓ and 9ℓ sublevels of Ar VIII, which are preferentially populated by the single electron capture process. A small but not negligible effect is seen for the experimental polarization ratios relating to transitions from sublevels of large ℓ values, showing a slight increase of the component parallel to the incident ion beam as the projectile energy increases. Theoretical polarization ratios obtained from CTMC calculated m_ℓ distributions are in excellent agreement with the measured polarization ratios. Electronic energy curve calculations are then presented in order to discuss these results in terms of dynamical couplings. [S1050-2947(97)02402-5]

PACS number(s): 34.10.+x

I. INTRODUCTION

Studying charge exchange is of considerable interest, in particular, to understand energy-loss processes in fusion plasmas [1]. Indeed, low-energy collisions between impurities (such as A^{q+} multicharged ions) and hydrogen atoms give rise to radiative emission which has been explained as due to the decay of $A^{(q-1)+}$ excited ions produced by the single-electron-capture process. Experimental and theoretical studies [2,3] have been devoted to the determination of the distributions of the excited ionic states produced during such collisions. From a theoretical point of view, collisions between bare ions and hydrogen targets are the simplest systems to study single-electron capture processes because they involve only one active electron. Experimentally, they are very difficult to work out. A mean to face this problem consists in studying collisions between partially stripped projectiles with a full-shell core and alkali-metal atom targets. We have then chosen to study collisions between $Ar^{8+}(2p^6)$ ions and Li($2s$) atoms.

We have already published [4–7] experimental and theoretical results concerning electron capture following Ar^{8+}-Li($2s$) collisions. They were experimentally studied for impact energies between 1.5 keV amu^{-1} (60 keV) and 4.5 keV amu^{-1} (180 keV) [5–7] by means of near UV and visible photon emission spectroscopy (200–600 nm). In this case, $n=8$ and $n=9$ levels are preferentially populated by single-electron-capture process and cross sections for capture into 8ℓ ($\ell=0$ to 7) and 9ℓ ($\ell=0$ to 8) sublevels were experimentally determined. Experimental 8ℓ and 9ℓ distributions were in good agreement with theoretical cross sections calculated by using the three-body classical trajectory Monte Carlo (CTMC) method. A strong selectivity in the ℓ distributions was observed and interpreted as the consequence of the competition between the Stark effect due to the electric field of the ionized target [8] and the projectile-core electron effect [9]. Explicitly, it was found that electron capture preferentially takes place into sublevels such as $\ell \geqslant 5$ (consequence of the Stark mixing effect) and, to a lesser extent, into sublevels with $\ell=0$, 1 (consequence of the projectile-core electron effect). The evolution of the $n\ell$ distributions with the collision energy has shown that the projectile-core electron effect was much stronger at low energy than at large energy [6,7].

In order to have a more complete characterization of the final states of capture, it is interesting, as suggested by Salin [10], to determine the m_ℓ distributions of the final states. Indeed, according to calculations made by Salin for monoelectronic systems (C^{6+}, O^{8+} and Ne^{10+}-H($1s$)), the m_ℓ Zeeman sublevel distributions are more significant for the collision process itself than the final ℓ distributions because the postcollisional Stark effect due to the electric field of the residual H^+ ion mixes the degenerate or nearly degenerate ℓ levels. The ℓ distributions are then deduced from the m_ℓ distributions assuming a complete equirepartition of the m_ℓ populations among the different ℓ levels. Moreover, recent CTMC calculations have given interesting results showing that the presence of the projectile-core electrons has an influence on the m_ℓ Zeeman sublevel populations [6]. A mean to experimentally estimate these m_ℓ distributions, i.e., the degree of alignment of the produced states, is to analyze the polarization of the emitted lines.

In a recent paper [11], we have presented results concerning polarization degree measurements of lines emitted during 80 keV Ar^{8+}-Li($2s$) collisions. In this experiment, the polarization degrees of lines corresponding to $7\ell'$-8ℓ and $8\ell'$-9ℓ transitions were measured. It was found that lines involving transitions from sublevels with low ℓ values ($7\ell'$-8ℓ and $8\ell'$-9ℓ with $\ell=0,1,2$) are unpolarized, within the experimental uncertainties. On the other hand, the

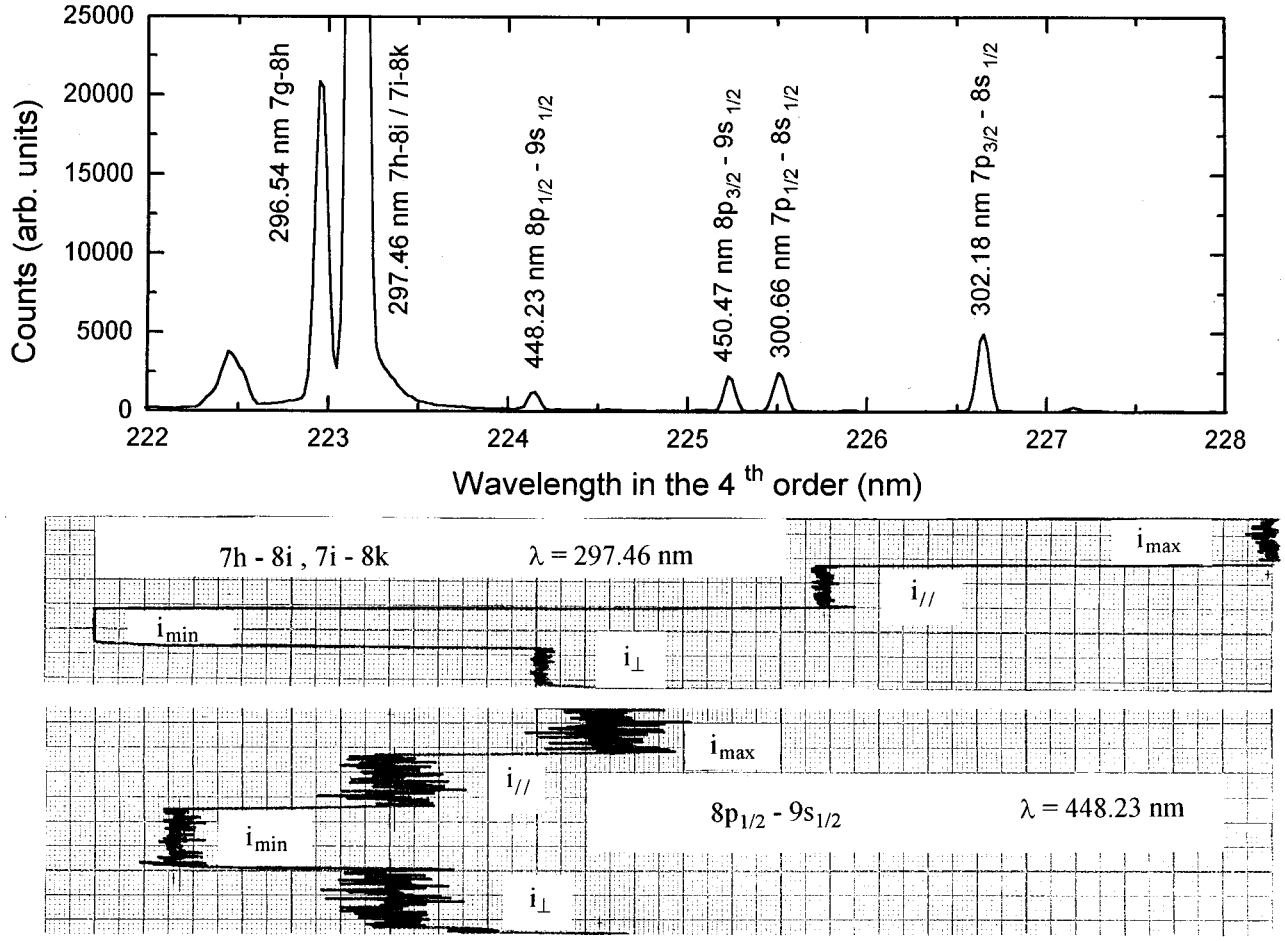

FIG. 1. Part of Ar^{8+}-Li spectrum (1.5 keV amu^{-1}) in the range 222–228 nm in the fourth order. Recordings of $7h$-$8i$, $7i$-$8k$, and $8p_{1/2}$-$9s_{1/2}$ line intensities for two polarization directions.

lines corresponding to transitions from sublevels of large angular momentum ($\ell \geq 4$) were found to be strongly polarized parallel to the incident ion-beam direction, the polarization degree increasing with increasing ℓ values. Qualitatively, these results show up a strong selectivity of the m_ℓ distributions which is confirmed by CTMC calculations of $\sigma(n\ell m_\ell)$ capture cross sections [11]. The polarization degrees calculated from these CTMC m_ℓ distributions were in good agreement with the experimental results. It allowed us to assert that sublevels with low m_ℓ values ($m_\ell = 0, \pm 1, \pm 2$) are preferentially populated by single capture process for a projectile energy of 2 keV amu^{-1} (80 keV).

Following our previous paper, the evolution of the m_ℓ distributions is now studied experimentally for collision energies from 1.5 keV amu^{-1} (60 keV) to 4.5 keV amu^{-1} (180 keV), and theoretically from 1 keV amu^{-1} (40 keV) to 4 keV amu^{-1} (160 keV). The experimental results will be discussed by comparison with theoretical polarization degrees obtained with $\sigma(n\ell m_\ell)$ capture cross sections calculated by using the CTMC method. Finally, a qualitative analysis based on electronic energy curve calculations will be proposed.

II. POLARIZATION MEASUREMENTS

A. Experimental setup

The experimental setup used here has already been described in detail [4–7]. The Ar^{8+} ion beam was produced by an electron cyclotron resonance (ECR) source at the GANIL (Grand Accélérateur National d'Ions Lourds, Caen, France) test bench. Photons emitted during Ar^{8+}-Li($2s$) collisions were detected for various projectile energies in the direction perpendicular to the Ar^{8+} beam and the Li jet. They were wavelength selected by a grating spectrometer (SOPRA 700) in the 200–600 nm range. The polarization of each line corresponding to $7\ell'$-8ℓ and $8\ell'$-9ℓ transitions was measured using a polarimeter composed of two polarizers [11]. The first one is a dichroic polarizer (Polacoat) which can be oriented parallel or perpendicular to the direction of the incident ion beam in order to measure the intensity of the emitted light polarized parallel ($I_\parallel$) or perpendicular ($I_\perp$) to the ion-beam direction. The second polarizer is a Glan-Taylor prism placed in front of the entrance slit of the spectrometer and fixed at 45° to the ion-beam direction in order to compensate for the polarization effects of the grating.

The polarization degree of a line is defined as

$$P = \frac{I_\parallel - I_\perp}{I_\parallel + I_\perp}.$$

A part of a typical Ar^{8+}-Li spectrum ($E = 1.5$ keV amu^{-1}) is presented in Fig. 1 together with some polarization recordings. The intensities recorded for two polarization directions are denoted $i_\parallel$ and $i_\perp$. They are referred to $i_{\min}$

which is obtained by crossing both polarizers. The emitted line intensities $I_{\parallel}$ and $I_{\perp}$ are then defined, respectively, as $(i_{\parallel}-i_{\min})$ and $(i_{\perp}-i_{\min})$. At last, $i_{\max}$ is obtained with polarizers parallel to each other.

The experimental uncertainties were evaluated from the recordings of $I_{\parallel}$ and $I_{\perp}$. The uncertainties due to the alignment defects of the experimental setup are very difficult to evaluate. However, preliminary tests with depolarized light of a mercury lamp have shown that they could be neglected in comparison with those deduced from the recordings.

B. Experimental results

The experimental polarization values are presented as a function of the collision energy in Table I, for each detected line corresponding to $7\ell'$-8ℓ and $8\ell'$-9ℓ transitions. For a given energy, the general tendency previously observed in [11] is conserved, i.e., 9ℓ and 8ℓ-sublevel decay lines are unpolarized or very weakly polarized for low angular momenta ($\ell=0,1,2$), whereas for $\ell\geqslant 4$, the polarization increases with increasing ℓ values.

In the investigated energy range and for a given $n'\ell'$-$n\ell$ transition, the evolution of the polarization degree remains moderate and depends on the ℓ value of the upper sublevel: on one hand, sublevels with low ℓ values ($\ell=0,1,2$) give rise constantly to unpolarized radiative emission, within the error bars; on the other hand, the polarization of radiative transitions from sublevels with large angular momenta ($\ell\geqslant 4$) is found to increase with incident energy. The increase of the polarization degrees is less important as the ℓ value increases. Moreover, the energy dependence is stronger for $7\ell'$-8ℓ transitions than for $8\ell'$-9ℓ transitions.

These observations are quite similar to those reported by Gauntt and Danzmann [12] for Ar^{8+}-Na($3s$) system in the 0.04–0.06 a.u. velocity range (0.04–0.09 keV amu^{-1}) and Schippers *et al.* [13] for He^{2+}-Na($3s$) system in the 2–13.3 keV amu^{-1} energy range. Indeed, Gauntt and Danzmann observed a slight increase of the polarization of $n'=8-n=9$ transition of Ar VIII with increasing velocity (from 15 to 20%), and Schippers *et al.* have found that the polarization of $n'=3-n=4$ transition of He II increases from 20 to 30% between 2 and 4 keV amu^{-1} and remains constant for $E>4$ keV amu^{-1}.

III. ZEEMAN SUBLEVEL DISTRIBUTIONS

A. Polarization and Zeeman sublevel distributions

The polarization degree of a line can be expressed as a function of the m_{ℓ} distributions of the decaying level, taking the ion-beam direction as quantization axis. Considering the transition from the $|\gamma J\rangle$ level to the $|\gamma' J'\rangle$ level, the intensities $I_{\parallel}$ and $I_{\perp}$ are related to the σ_{JM_J} Zeeman sublevel populations as

$$I_{\parallel}\propto \sum_{\substack{M_J,M'_{J'}\\ M_J=M'_{J'}}} \begin{pmatrix} J & 1 & J' \\ -M_J & 0 & M'_J \end{pmatrix}^2 \sigma_{JM_J}$$

and

$$I_{\perp}\propto \sum_{\substack{M_J,M'_{J'}\\ M_J=M'_{J'},\pm 1}} \begin{pmatrix} J & 1 & J' \\ -M_J & \pm 1 & M'_J \end{pmatrix}^2 \sigma_{JM_J}.$$

The σ_{JM_J} Zeeman sublevel populations are related to the $\sigma_{m_{\ell}m_s}$ populations in the following way:

$$\sigma_{JM_J}=\sum_{\substack{m_{\ell},m_s\\ m_{\ell}+m_s=M_J}} |\langle \gamma \ell s m_{\ell} m_s|JM_J\rangle|^2 \sigma_{m_{\ell}m_s}.$$

The target is not prepared in a magnetic oriented state, so $\sigma_{m_s}=\sigma_{-m_s}$, and the ion beam is a symmetry axis for the experiment, so $\sigma_{m_{\ell}}=\sigma_{-m_{\ell}}=\sigma_{|m_{\ell}|}$.

If $\ell\geqslant 3$, the wavelengths of the three fine-structure transitions $^2L'_{J'}$-^2L_J are very close and the corresponding lines are no longer resolved by the optical device. As the L-S coupling is negligible in this case, Fano and Macek formalism [14] was used to determine the polarization degree of each $n'\ell'$-$n\ell$ transition. The polarization is then expressed as

$$P(n'\ell'\text{-}n\ell)=\frac{3h(\ell',\ell)A(\ell)}{4+h(\ell'\ell)A(\ell)},$$

where $A(\ell)$ is the alignment parameter of the ℓ upper level

$$A(\ell)=-p(0)+2\sum_{m_{\ell}=1}^{\ell}\frac{3m_{\ell}^2-\ell(\ell+1)}{\ell(\ell+1)}p(m_{\ell}),$$

where

$$p(0)=\frac{\sigma_0}{(\sigma_0+2\Sigma_{m_{\ell}=1}^{\ell}\sigma_{m_{\ell}})}$$

and

$$p(m_{\ell})=\frac{\sigma_{m_{\ell}}}{(\sigma_0+2\Sigma_{m_{\ell}=1}^{\ell}\sigma_{m_{\ell}})}$$

and

$$h(\ell',\ell)=(-1)^{\ell-\ell'}\begin{Bmatrix} \ell & \ell & 2 \\ 1 & 1 & \ell' \end{Bmatrix}\begin{Bmatrix} \ell & \ell & 2 \\ 1 & 1 & \ell \end{Bmatrix}^{-1}.$$

Theoretical polarization values can then be obtained from these final expressions and from $\sigma(n\ell m_{\ell})$ capture cross sections (also denoted $\sigma_{m_{\ell}}$). In all cases, it leads to a final expression of the polarization degree P as a function of the $\sigma_{m_{\ell}}$ populations of the upper level in the form

$$P=\frac{a_0\,\sigma_0+a_1\,\sigma_1+a_2\,\sigma_2+\cdots+a_{\ell-1}\sigma_{\ell-1}+a_{\ell}\,\sigma_{\ell}}{b_0\,\sigma_0+b_1\,\sigma_1+b_2\,\sigma_2+\cdots+b_{\ell-1}\sigma_{\ell-1}+b_{\ell}\,\sigma_{\ell}} \quad (1)$$

where the $a_{m_{\ell}}$ and $b_{m_{\ell}}$ coefficients result either from the calculation of $I_{\parallel}$ and $I_{\perp}$ and the change of basis $|\ell s J\, M_J\rangle\rightarrow|\ell s m_{\ell}\, m_s\rangle$ (transitions $^2L'_{J'}$-^2L_J) or from the

TABLE I. Experimental polarization rates (%) vs the projectile energy (keV amu^{-1}) for lines corresponding to the $7\ell'$-8ℓ and $8\ell'$-9ℓ transitions.

Energy Transition	1.5	2.0	2.5	3.0	3.5	4.0	4.5
$7p_{1/2}$-$8s_{1/2}$	-1.4 ± 5.2	-2.3 ± 5.0	0.0 ± 5.0	0.0 ± 5.8	-1.3 ± 6.0	-0.5 ± 6.0	2.8 ± 6.8
$7p_{3/2}$-$8s_{1/2}$	-1.4 ± 5.5	-0.2 ± 3.0	-0.3 ± 5.0	-0.6 ± 6.4	-1.7 ± 5.2	-0.3 ± 6.0	0.5 ± 3.8
$7d_{3/2}$-$8p_{1/2}$	-0.9 ± 2.8	-2.6 ± 2.6	-0.7 ± 2.7	-2.5 ± 3.8	-0.6 ± 6.7	1.7 ± 5.9	-1.3 ± 5.0
$7d_{5/2}$-$8p_{3/2}$	1.9 ± 2.5	1.8 ± 2.4	5.2 ± 5.2	3.2 ± 2.0	4.1 ± 3.6	6.5 ± 3.7	5.9 ± 4.4
$7f$-$8d$	-4.9 ± 8.0	-1.3 ± 5.0	2.6 ± 7.8	1.1 ± 6.8	-1.5 ± 9.0	-1.7 ± 6.0	[a]
$7f$-$8g$	6.5 ± 2.6	11.7 ± 2.6	16.0 ± 3.8	16.8 ± 2.8	18.3 ± 3.5	18.9 ± 3.4	20.7 ± 3.7
$7g$-$8h$	13.3 ± 2.4	17.3 ± 1.5	20.2 ± 1.0	21.5 ± 0.9	23.8 ± 1.9	24.3 ± 2.9	25.3 ± 2.1
$7h$-$8i$/$7i$-$8k$	23.3 ± 2.6	25.0 ± 1.8	26.2 ± 1.3	27.9 ± 1.8	29.4 ± 3.0	29.1 ± 2.6	28.8 ± 1.0
$8p_{1/2}$-$9s_{1/2}$	0.0 ± 9.0	1.7 ± 4.6	2.5 ± 5.7	-2.2 ± 4.3	[a]	[a]	[a]
$8p_{3/2}$-$9s_{1/2}$	-0.3 ± 2.6	-1.6 ± 2.6	-0.6 ± 3.2	-1.2 ± 4.8	2.1 ± 5.0	3.7 ± 7.0	3.0 ± 9.0
$8f$-$9g$	19.6 ± 2.6	22.1 ± 4.6	24.0 ± 4.1	22.0 ± 3.4	23.9 ± 3.9	24.2 ± 4.1	25.8 ± 5.3
$8g$-$9h$	23.3 ± 2.3	25.1 ± 1.4	26.0 ± 1.0	28.8 ± 2.5	27.9 ± 2.7	28.1 ± 2.4	27.9 ± 0.8
$8h$-$9i$/$8i$-$9k$/$8k$-$9l$	28.0 ± 3.3	28.2 ± 2.8	29.4 ± 2.8	30.0 ± 1.9	30.0 ± 2.5	30.0 ± 2.1	29.1 ± 3.0

[a]The intensity of this line was too weak.

calculation of the alignment parameter and the quantity $h(\ell',\ell)$ (transitions $n'\ell'$-$n\ell$). For $n'\ell'$-$n\ell$ transitions, the a_{m_ℓ} coefficients are found to be positive for $|m_\ell| \leqslant \mathrm{Int}[(\ell+1)/2]$ and negative for $|m_\ell| > \mathrm{Int}[(\ell+1)/2]$, whereas the b_{m_ℓ} coefficients are always positive.

It is obvious that the polarization measurements alone cannot lead to the determination of the experimental Zeeman sublevel populations for the following reason: as soon as $\ell \geqslant 2$, the number of magnetic sublevel populations to calculate is higher than the number of equations to solve [11]. However, the above considerations on the signs of a_{m_ℓ} and b_{m_ℓ} coefficients and the high positive experimental polarization degrees ($P \cong 20$–30%) indicate that magnetic sublevels with low m_ℓ values are preferentially populated by the single-electron-capture process.

Moreover, it is worth noting that the m_ℓ populations probably do not vary significantly between 1.5 and 4.5 keV amu^{-1} since the experimental polarization degrees are not strongly energy dependent.

B. CTMC Zeeman sublevel distributions

In order to have more complete informations on the magnetic sublevel distributions and on their energy dependence, cross sections for capture into the different $n\ell m_\ell$ sublevels were calculated by using the CTMC method [11]. Theoretical polarization values were then deduced from these m_ℓ distributions and were compared with our measurements.

The CTMC method is based on solving the Hamiltonian equations for the motion of a three-body system (the valence electron, the Li^+ alkali-metal core, and the Ar^{8+} ionic projectile) given a set of initial conditions for the projectile and the target [15,16]. Details on the CTMC method concerning the use of effective electron-core interactions can be found elsewhere [17,18]. Model potentials were used to describe the interactions between the valence electron and the ionic cores Li^+ and Ar^{8+}, their analytic form, and their parameters are given in Refs. [4] and [7]. The quantum defects of the atomic energy levels of the Ar^{7+} ion [19] were also taken into account in the determination of the final $n\ell m_\ell$ distributions. For every trajectory ending in the electron-capture process, the final quantum numbers n, ℓ, and m_ℓ were determined through a binning procedure of the classical quantities (electronic energy, electronic angular momentum, and its projection along the direction of initial velocity taken as quantization axis) which has already been described in Refs. [4] and [11]. A large number of trajectories (between 7.5×10^4 and 1.25×10^5, depending on the collision energy) was used to insure statistical errors less than 10% for the most populated $n\ell m_\ell$ sublevels.

The CTMC m_ℓ distributions are reported in Table II for the 8ℓ sublevels and in Table III for the 9ℓ sublevels, in the range 1–4 keV amu^{-1}. For a given energy, the distributions of the relative capture cross sections are peaked on low m_ℓ values ($m_\ell = 0, \pm1, \pm2$), the populations decreasing roughly as $|m_\ell| \geqslant 3$. In the considered energy range, and for sublevels with large ℓ values ($\ell \geqslant 4$), the populations of $m_\ell = 0, \pm1, \pm2$ sublevels increase very weakly with increasing energies, and the energy dependence of the m_ℓ populations completely vanishes for $\ell = 7,8$.

For sublevels with low ℓ values ($\ell = 0,1,2,3$), the percentages of magnetic sublevels of $m_\ell = 0$ ($\ell = 1,2,3$) and $m_\ell = \pm1$ ($\ell = 2,3$) increase significantly with increasing energies, showing a clear projectile velocity effect on the alignment of these states. At last, for a given ℓ value, the Zeeman populations are more selective and vary more slowly for 9ℓ sublevels than for 8ℓ sublevels. The relative uncertainties on the CTMC cross sections are of 5 to 10% for the most populated sublevels.

The polarization degrees and the corresponding uncertainties were calculated from these m_ℓ distributions. For transitions from sublevels with $\ell \geqslant 2$, the calculations were improved by including radiative cascade effects following the method of Lin and Macek [20] and neglecting transitions with $\Delta\ell = \ell - \ell' = -1$ for which branching ratios are very small. We have considered $10\ell'' \rightarrow 9\ell$ cascades for $9\ell \rightarrow 8\ell'$ transitions, and $10\ell'' \rightarrow 8\ell$ and $10\ell'' \rightarrow 9\ell'' \rightarrow 8\ell$ cascades for $8\ell \rightarrow 7\ell'$ transitions. The

TABLE II. CTMC m_ℓ distributions (%) vs the projectile energy (keV amu^{-1}) for single-electron capture into 8ℓ sublevels during Ar^{8+}-Li($2s$) collisions.

	Energy							
	m	1.0	1.5	2.0	2.5	3.0	3.5	4.0
$8s$	0	100	100	100	100	100	100	100
$8p$	0	20.3	23.8	26.4	27.7	32.0	35.0	39.2
	±1	39.9	38.1	36.8	36.2	34.0	32.5	30.4
$8d$	0	19.3	19.1	18.8	22.0	21.9	25.6	26.4
	±1	18.2	18.8	20.8	21.9	21.2	22.4	23.1
	±2	22.2	21.6	19.8	17.1	17.8	14.8	13.7
$8f$	0	14.6	14.8	17.0	16.8	19.5	21.2	23.4
	±1	14.3	14.8	14.1	16.0	19.7	19.2	19.2
	±2	14.0	13.9	16.1	13.6	12.7	12.5	12.5
	±3	14.5	13.9	11.3	12.0	7.8	7.7	6.6
$8g$	0	14.2	13.5	16.6	14.1	16.6	17.9	16.8
	±1	13.0	13.1	14.6	14.6	13.6	14.7	16.4
	±2	11.2	12.2	13.5	13.9	14.6	13.4	13.4
	±3	9.3	11.3	8.8	9.1	9.4	9.5	9.3
	±4	9.4	6.7	4.8	5.3	4.0	3.5	2.5
$8h$	0	12.5	12.3	11.8	13.5	13.0	15.1	15.8
	±1	12.5	12.9	12.7	12.4	12.9	13.8	15.2
	±2	10.7	10.7	11.6	11.6	13.2	13.1	12.8
	±3	9.2	10.2	9.5	9.7	9.8	8.4	8.6
	±4	7.2	6.8	7.2	6.1	4.8	5.3	4.3
	±5	4.2	3.3	3.1	3.4	2.8	1.9	1.2
$8i$	0	11.9	12.8	12.2	12.4	14.0	13.9	13.8
	±1	11.2	12.5	12.9	13.7	13.0	13.1	13.5
	±2	9.9	10.1	10.9	11.9	12.4	12.5	12.7
	±3	9.3	8.1	9.0	8.3	9.1	10.3	9.5
	±4	6.3	6.4	6.2	5.3	4.9	4.7	5.3
	±5	4.5	4.0	2.4	2.3	2.0	1.5	1.3
	±6	2.9	2.6	2.5	2.3	1.6	1.0	0.7
$8k$	0	12.9	14.0	13.6	14.3	14.1	13.7	13.2
	±1	12.2	13.0	13.4	14.1	13.9	13.2	13.3
	±2	10.0	11.5	12.6	11.6	11.7	12.0	12.1
	±3	7.3	7.5	8.1	9.0	9.3	9.9	9.8
	±4	4.9	4.4	4.4	5.0	5.4	6.0	6.0
	±5	3.6	2.7	2.2	1.7	1.7	1.6	1.7
	±6	3.3	2.1	1.5	0.7	0.4	0.2	0.2
	±7	2.2	1.9	1.0	0.7	0.5	0.3	0.3

TABLE III. CTMC m_ℓ distributions (%) vs the projectile energy (keV amu^{-1}) for single-electron capture into 9ℓ sublevels during Ar^{8+}-Li($2s$) collisions.

	Energy							
	m	1.0	1.5	2.0	2.5	3.0	3.5	4.0
$9s$	0	100	100	100	100	100	100	100
$9p$	0	31.6	40.6	39.8	43.3	46.2	52.6	54.1
	±1	34.2	29.7	30.1	28.4	26.9	23.7	23.0
$9d$	0	27.7	32.9	31.2	31.0	31.4	30.6	32.9
	±1	23.8	23.4	25.1	23.8	25.0	28.6	26.8
	±2	12.3	10.1	9.3	10.7	9.3	6.1	6.7
$9f$	0	24.3	24.9	25.6	26.6	25.5	30.2	28.3
	±1	19.8	21.3	21.7	23.7	24.4	23.1	24.5
	±2	12.8	12.0	11.6	11.3	11.2	10.6	9.6
	±3	5.5	4.3	3.9	1.7	1.7	1.2	1.7
$9g$	0	22.1	23.5	20.2	22.5	23.3	20.2	21.1
	±1	19.3	19.8	19.8	18.6	18.5	19.7	19.6
	±2	12.3	12.7	12.5	13.8	13.1	12.8	13.0
	±3	5.1	4.9	6.4	5.7	6.0	6.8	6.4
	±4	2.3	0.8	1.2	0.7	0.8	0.6	0.4
$9h$	0	19.9	20.6	18.4	19.8	20.7	19.2	21.0
	±1	18.2	18.5	17.4	17.9	18.4	18.5	19.2
	±2	11.8	12.1	13.4	12.9	11.6	12.9	11.5
	±3	6.6	6.4	6.7	6.1	5.8	6.1	6.3
	±4	2.7	2.4	2.8	2.7	3.2	2.5	2.3
	±5	0.8	0.4	0.5	0.5	0.6	0.4	0.2
$9i$	0	20.2	19.5	16.8	18.0	18.1	19.0	19.5
	±1	17.1	17.5	16.8	17.3	17.7	18.3	18.2
	±2	11.4	12.1	13.8	12.8	13.3	14.1	14.4
	±3	6.5	6.5	7.1	7.0	6.6	5.6	5.7
	±4	2.7	2.7	2.2	2.5	2.2	1.7	1.4
	±5	1.5	1.1	1.1	1.0	0.9	0.6	0.4
	±6	0.7	0.3	0.6	0.4	0.3	0.2	0.1
$9k$	0	18.5	18.5	18.0	16.9	15.5	15.6	15.1
	±1	16.9	16.1	16.6	16.5	16.3	16.2	16.4
	±2	11.3	12.6	13.4	13.8	14.9	15.0	15.1
	±3	5.6	6.9	6.8	7.6	8.1	8.2	8.0
	±4	3.4	2.7	2.4	2.3	2.1	2.1	2.3
	±5	1.8	1.5	0.9	0.7	0.5	0.4	0.3
	±6	1.5	0.8	0.6	0.4	0.3	0.2	0.2
	±7	0.3	0.2	0.3	0.2	0.1	0.1	0.1
$9l$	0	17.3	18.9	17.2	17.6	16.8	16.9	16.0
	±1	14.7	16.4	17.7	17.0	16.0	16.1	16.5
	±2	10.3	11.9	12.7	13.6	14.8	14.8	14.7
	±3	6.1	5.6	6.5	7.3	8.0	8.0	8.0
	±4	4.5	2.9	2.3	1.9	1.9	2.0	2.0
	±5	2.5	1.9	1.2	0.6	0.4	0.3	0.3
	±6	1.9	1.2	0.6	0.4	0.2	0.2	0.1
	±7	1.1	0.6	0.3	0.3	0.2	0.1	0.2
	±8	0.4	0.1	0.1	0.1	0.1	0.1	0.1

cascade effects were found to be depolarizing for transitions from $n=9$ whereas the polarization degrees of transitions from $n=8$ sublevels were slightly enhanced because of alignment transfer from $n=9$ levels. But in general, the cascade effects were found to be weak and did not affect strongly the calculated polarization values.

The results of measurements and calculations including cascade effects are reported in Figs. 2(a)–(e) for $7\ell'$-8ℓ transitions and in Figs. 3(a)–(c) for $8\ell'$-9ℓ transitions, with the exception of $7p_{1/2,3/2}$-$8s_{1/2}$, $7d_{3/2}$-$8p_{1/2}$, and $8p_{1/2,3/2}$-$9s_{1/2}$ lines which were detected unpolarized, as it was theoretically expected. For transitions involving sublevels with large ℓ values (i.e., $\ell \geqslant 4$), the polarization degrees calculated including the cascades are higher than the experimental polarization values, but in the worse cases, the calculations hardly stand out of the experimental error bars. As a first observation, the theoretical polarization degrees vary more softly with the collision energy than the experimental ones. If we except some small discrepancies in the 1–2 keV amu^{-1} energy range and concerning more specifically $7f$-$8g$ and $8f$-$9g$ transitions (for which the theoretical po-

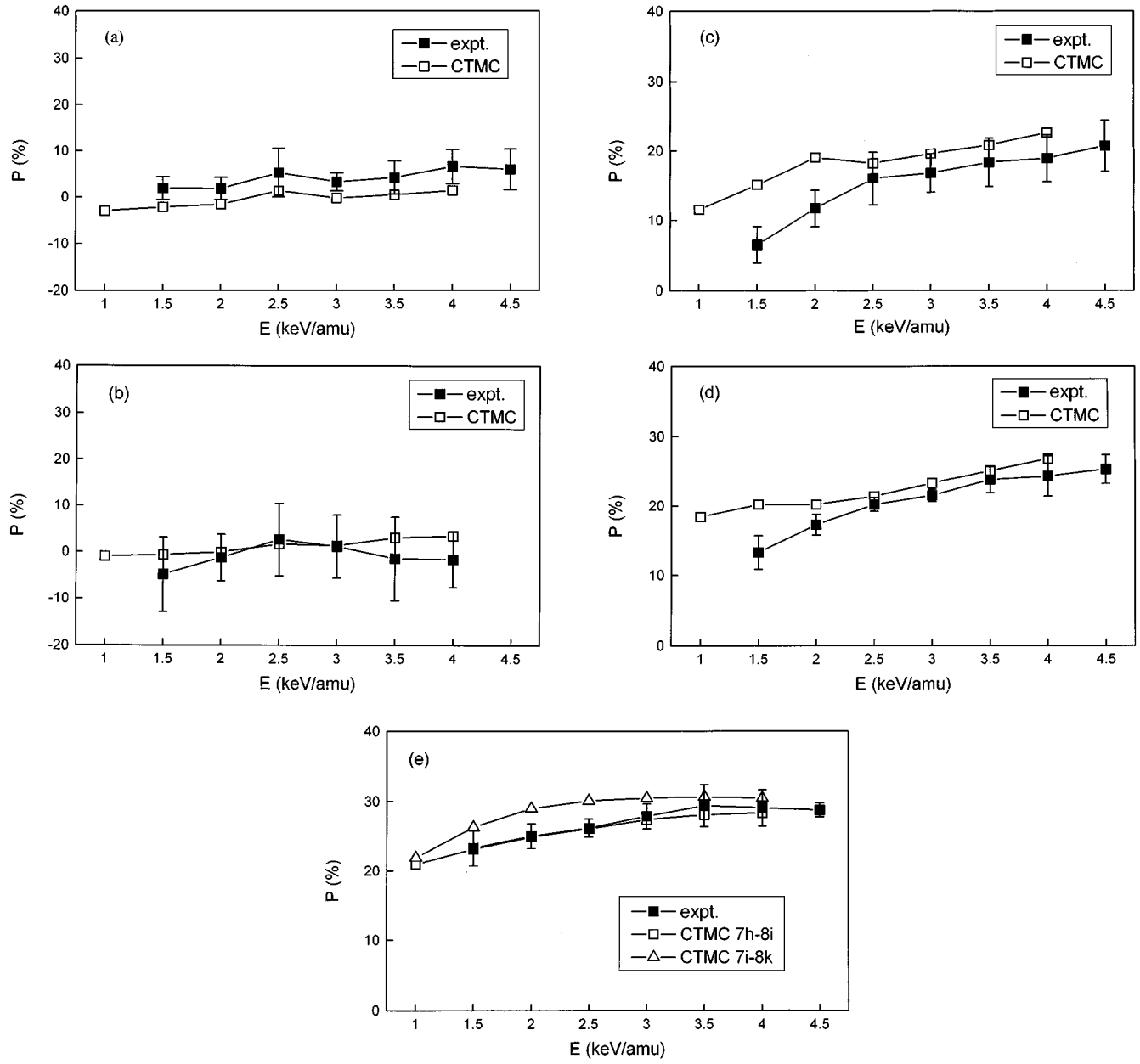

FIG. 2. Experimental and theoretical polarization degrees of lines corresponding to $7\ell'$-8ℓ transitions vs the projectile energy between 1.5 keV amu^{-1} and 4.5 keV amu^{-1}. (a) $7d_{5/2}$-$8p_{3/2}$, (b) $7f$-$8d$, (c) $7f$-$8g$, (d) $7g$-$8h$, and (e) $7h$-$8i$ and $7i$-$8k$ (the solid squares are related to both transitions, the open squares, and the open triangles are related, respectively, to $7h$-$8i$ and $7i$-$8k$ transitions).

larization degrees do not decrease significantly at low energy, as was experimentally found), we observe a good agreement between the calculated and the experimental results, showing that the CTMC method is suitable to predict the m_ℓ distributions.

C. Zeeman sublevel distributions and charge-exchange processes

1. Phenomenological approach

The m_ℓ distributions, and subsequently the polarization degrees, reflect both the primary collisional process and the postcollision process which depend in a complicated way on the relative importance of radial and rotational couplings, of Stark mixing and projectile-core electron effects.

According to calculations made by Salin [10] for monoelectronic systems (i.e., C^{6+}, O^{8+}, and Ne^{10+}-H($1s$)), only $m_\ell=0$ magnetic sublevels are produced during the primary capture process. Therefore, the population of $m_\ell\neq 0$ sublevels is due to postcollisional effects (i.e., the Stark mixing and the rotational coupling). In our case, the presence of the projectile-core electrons, and more specifically, the competition between the Stark mixing effect and the projectile-core electron effect must be taken into account. The projectile core lifts the degeneracy of the hydrogenic low ℓ states ($\ell<4$), and only the high ℓ states ($\ell\geqslant 4$) may be affected by the Stark effect which mixes the degenerate or nearly degenerate $n\ell$ sublevels.

The effect of the projectile-core electrons on the polarization of the emitted lines has already been studied experimen-

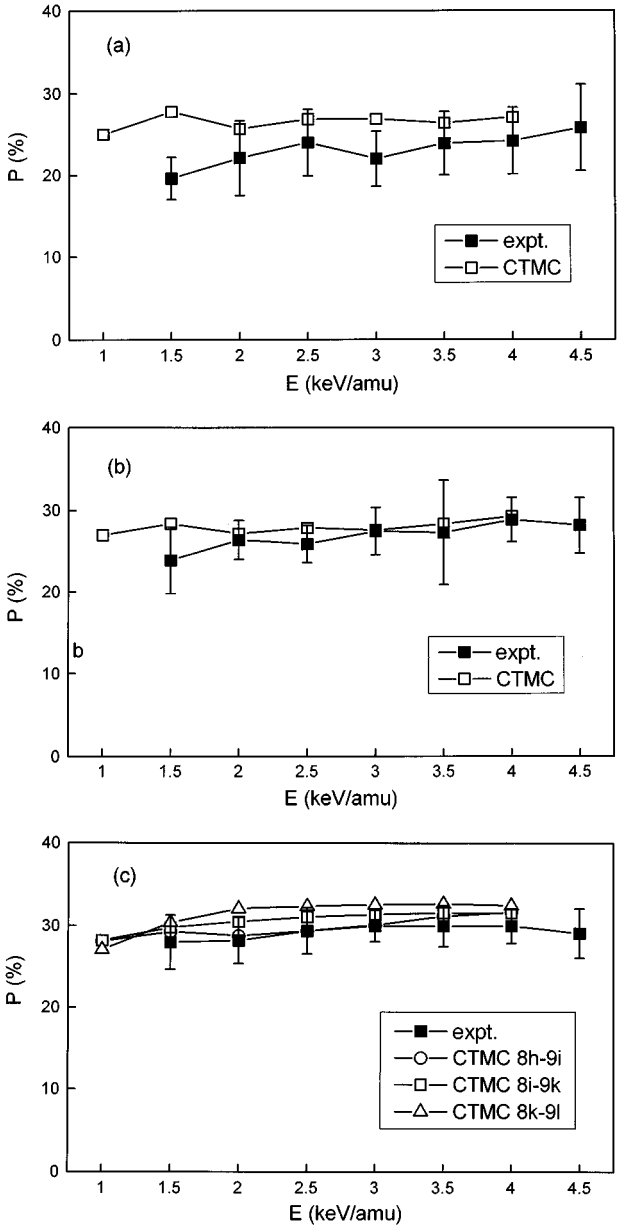

FIG. 3. Experimental and theoretical polarization degrees of lines corresponding to $8\ell'$-9ℓ transitions vs the projectile energy between 1.5 keV amu^{-1} and 4.5 keV amu^{-1}. (a) $8f$-$9g$ transition, (b) $8g$-$9h$ transition, and (c) $8h$-$9i$, $8i$-$9k$, and $8k$-$9l$ transitions (the solid squares are related to the three transitions, the open circles, open squares, and open triangles are related, respectively, to $8h$-$9i$, $8i$-$9k$, and $8k$-$9l$ transitions).

tally by Lembo *et al.* [21] in the case of capture collisions between Na($3s$) and Ar^{8+} and Ne^{8+} ions. These experiments have shown that the core effect is depolarizing. The comparison between experimental and CTMC calculated polarization degrees obtained for Ar^{8+}-Li($2s$) collisions and those determined from CTMC calculations for O^{8+}-Li($2s$) collisions at energies of 2, 3, and 4 keV amu^{-1} (see Table IV) confirms this tendency. Indeed, the polarization of lines corresponding to transitions involving high ℓ values are seen to be almost the same for both collision systems, whereas the polarization degrees of radiative transitions involving low ℓ values are larger in the case of O^{8+}-Li($2s$) collisions than

TABLE IV. Theoretical polarization rates (%) vs the projectile energy (keV amu^{-1}) calculated from the CTMC m_ℓ distributions for O^{8+}-Li($2s$) collisions.

Energy Transition	2.0	3.0	4.0
$7p_{1/2}$-$8s_{1/2}$	0	0	0
$7p_{3/2}$-$8s_{1/2}$	0	0	0
$7d_{3/2}$-$8p_{1/2}$	0	0	0
$7d_{5/2}$-$8p_{3/2}$	2.4±1.2	2.7±1.7	3.7±1.3
$7f$-$8d$	4.9±1.5	7.4±1.6	8.6±1.0
[a]	4.0	5.8	6.7
$7f$-$8g$	25.8±1.8	26.2±1.8	28.8±1.0
[a]	25.1	26.2	28.4
$7g$-$8h$	25.9±1.3	28.3±1.2	28.4±0.7
[a]	26.9	29.0	29.4
$7h$-$8i$	26.7±1.1	27.6±0.9	27.1±0.5
[a]	28.8	29.8	29.5
$7i$-$8k$	27.8±0.9	28.9±0.7	29.0±0.5
[a]	30.2	31.4	31.3
$8p_{1/2}$-$9s_{1/2}$	0	0	0
$8p_{3/2}$-$9s_{1/2}$	0	0	0
$8f$-$9g$	31.3±1.8	33.5±1.8	35.2±0.9
[a]	29.3	31.5	32.6
$8g$-$9h$	31.0±1.3	33.7±0.9	34.4±1.1
[a]	29.7	32.3	33.1
$8h$-$9i$	32.3±0.8	33.2±0.6	33.8±0.3
[a]	31.3	32.3	32.9
$8i$-$9k$	32.6±1.1	32.9±0.4	32.8±0.2
[a]	32.0	32.4	32.3
$8k$-$9l$	32.5±0.6	33.7±0.3	33.7±0.2
[a]	32.2	33.3	33.4

[a]Calculations including the radiative cascade effects.

in the case of Ar^{8+}-Li($2s$) collisions. The differences are clearer in the case of capture into 8ℓ sublevels than for capture into 9ℓ sublevels, and are less important at 4 keV amu^{-1} than at 2 keV amu^{-1} for capture into 8ℓ sublevels. As a consequence, we have to distinguish two cases in the asymptotic evolution of the state alignment : the case of low ℓ states, which are strongly affected by the core effect, and the case of high ℓ states, which are sensitive to the Stark mixing.

The evolution of the polarization degrees with the collision energy depends on the evolution of the dynamical couplings with the projectile velocity. It is well established that radial and rotational couplings are linked, respectively, to the radial and angular relative velocities of the collision partners and that the projectile-core electron effect is also sensitive to the impact velocity. Thus, the combination of such different effects precludes any simple interpretation.

2. Electronic energy curve calculations

In order to substantiate these conclusions, we have calculated, by using a pseudopotential method (see the Appendix), the electronic energies of one-electron $(X^{7+}+\mathrm{Li})^+$ systems, where $X \equiv$ O, Ar. The core-core interaction (mainly the $8/r$ repulsive interaction) is not considered in the calculations

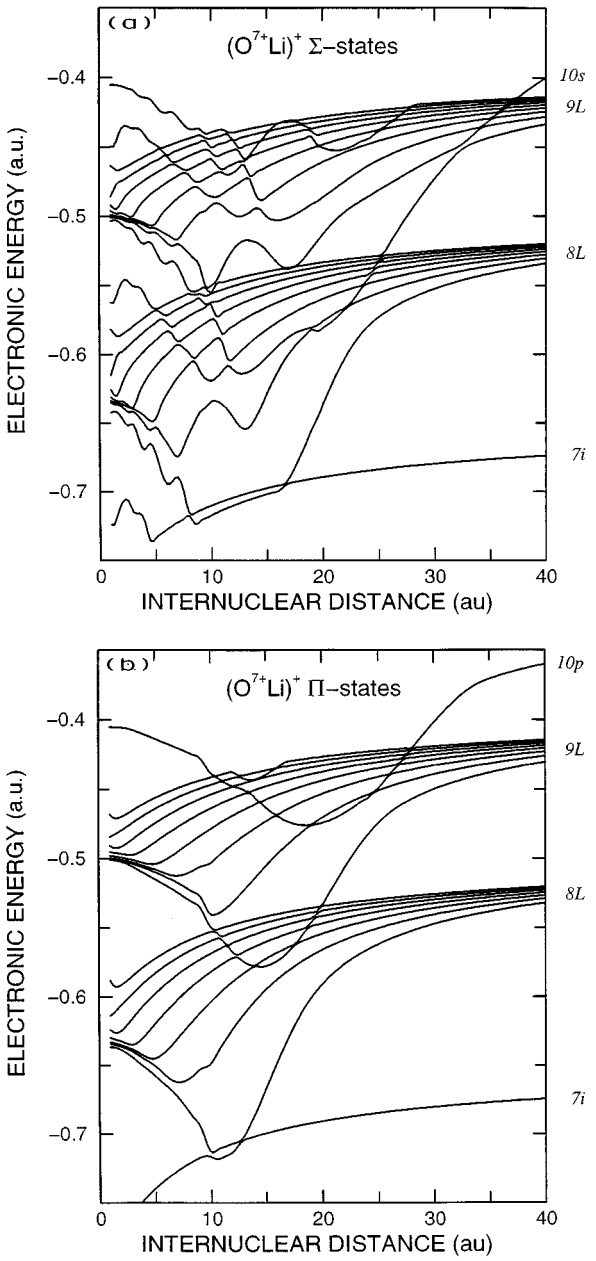

FIG. 4. Potential energy curves of $(O^{7+}+Li)^+$ system calculated in the internuclear distance range $R=1-40$ a.u. (a) Σ states, (b) Π states.

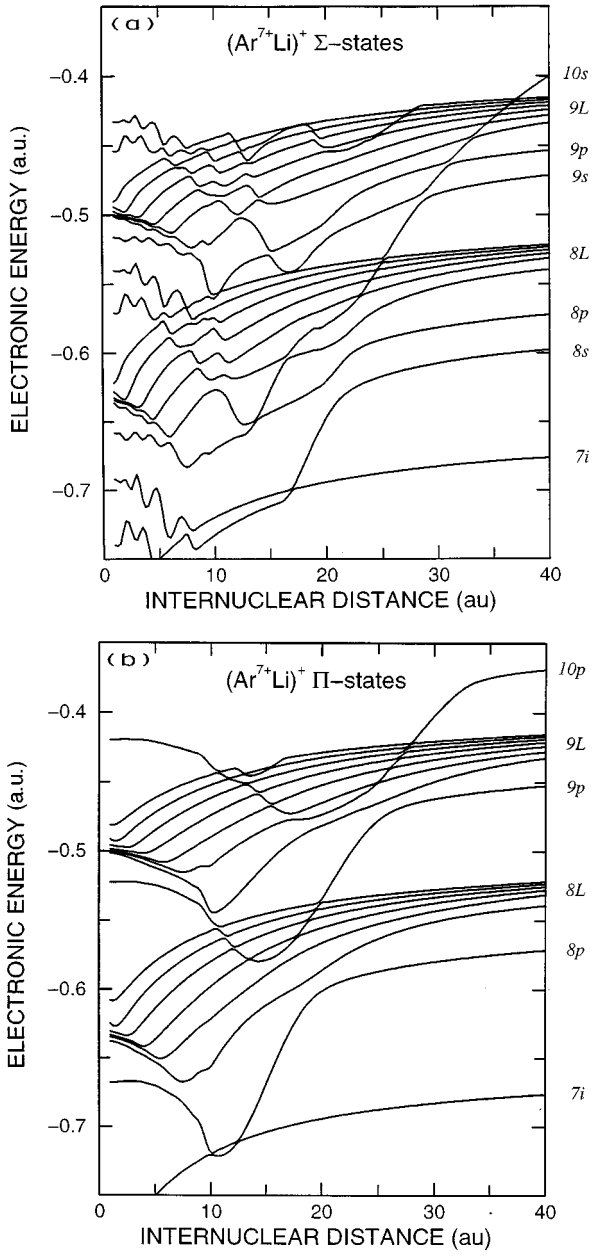

FIG. 5. Potential-energy curves of $(Ar^{7+}+Li)^+$ system calculated in the internuclear distance range $R=1-40$ a.u. (a) Σ states, (b) Π states.

since it does not contribute to the nonadiabatic couplings between the molecular states. For the internuclear distance range $R=1-40$ a.u., the electronic energies relevant to the capture into the levels $n=8$ and $n=9$ of X^{7+} are shown for the Σ and Π symmetries in Figs. 4(a) and 4(b) for the $(O^{7+}+Li)^+$ system, and in Figs. 5(a) and 5(b) for the $(Ar^{7+}+Li)^+$ system. The two electronic energy curves just above and just below the two manifolds of energy curves are also shown in the figures. In particular, the Σ energy curves just above the uppermost Σ energy curve correlating to the $n=9$ level of X^{7+} ion, and which goes to the $2s$ state of Li at large R values through numerous nearly diabatic crossings of Σ-energy curves, is the entrance channel for the electron-capture process. The electronic energies for the symmetries $\Lambda \geqslant 2$ have also been calculated, but are not of interest for the present discussion as varying too monotonously with R.

(a) $(O^{7+}+Li)^+$ *system.* Considering the $(O^{7+}+Li)^+$ system, two avoided crossings between the entrance Σ channel and the lowest Σ energy curve of each of the two manifolds of molecular channels correlating to the $n=8$ and 9 levels at large R values are clearly seen at $R\approx 22.5$ a.u. and $R\approx 32.4$ a.u., respectively. They are responsible for the primary radial couplings leading to populate, at larger R values, the 8ℓ and 9ℓ state manifolds by Stark effect of the residual Li^+ ion [10,18]. Beside these primary radial couplings, there are also primary rotational couplings between the Σ-entrance channel and the Π-energy curves of the electron-capture channels in the curve crossing regions, which therefore participate to populate directly the various ℓ levels at

large R values. These rotational couplings should be more effective at large than at low energies. In the absence of any other couplings, only the $m=0$ and ± 1 substates would be populated in the electron-capture process. However, beside these primary couplings, there are also intrashell ($\Delta\ell=0$) and intershell ($\Delta\ell\neq 0$) rotational couplings between the molecular states of a same manifold of electron-capture channels. Those successive rotational couplings (between molecular states with $\Delta\Lambda=\pm 1$) are responsible for populating predominantly large ℓ values, and for determining the final m distribution within a ℓ subshell at large R values.

(b) $(Ar^{7+}+Li)^{+}$ *system.* In the case of the $(\mathrm{Ar}^{7+}+\mathrm{Li})^{+}$ system, the degeneracy of the levels for $\ell\leqslant 2$ is removed by the presence of the core electrons in the separated atom limit. The results are that the Σ-electronic energy curves correlating to these levels show up avoided crossings with the entrance channel and among themselves in the region $R\approx 20$–23 a.u. for those correlating to the $n=8$ level, and $R\approx 28$–33 a.u. for those correlating to the $n=9$ level. These regions of radial couplings at the avoided crossings are responsible for the core-electron effect observed in Ar^{8+}-Li($2s$) collisions, where low ℓ values are populated in the electron-capture process [4–7]. The other Σ-energy curves correlating to capture levels with $\ell\geqslant 3$ show the similar Stark behavior than observed for the $(\mathrm{O}^{7+}+\mathrm{Li})^{+}$ system, at distances larger than at the crossing regions with the entrance channel.

At very high energies, all the avoided crossings become diabatic and no core-electron effect should be observed, as for O^{8+}-Li($2s$) collisions. *As the energy decreases*, it is the primary population of the molecular channels correlating to the $8s,8p,8d$ and $9s,9p,9d$ sublevels which should be responsible for populating 8ℓ and 9ℓ sublevels with large ℓ values, by Stark effect and rotational couplings, as for O^{8+}-Li($2s$) collisions. Comparatively, the avoided crossings associated with $n=8$ sublevels have much larger energy splittings than the corresponding ones associated with $n=9$. Therefore, as the energy decreases, the core-electron effect should manifest first in the final ℓ distribution of $n=8$ level, and at lower energies in the case of $n=9$ level. In the case of capture into 8ℓ levels with $\ell\leqslant 2$, various mechanisms by radial coupling may occur, which may complicate the electron-capture mechanisms. For example, the radial coupling may directly bring the electron from the Σ-entrance channel (presently, the Σ-electronic energy curve correlated to the $8f$ sublevel) to the Σ-molecular channel correlated to the $8s$ sublevel (noted Σ_{8s}). But it can also be done via the radial coupling from the entrance channel to the molecular channel Σ_{9p}, followed by the subsequent radial coupling to the capture channel Σ_{8s} (other possibilities exist also via the Σ_{9d} channel). Finally, the rotational couplings between the Σ-entrance channel and the Π-molecular channels can also populate directly the various $n\ell$ capture channels. These radial and rotational couplings should contribute to populate sublevels with $m=0$ and ± 1. But it is the subsequent intrashell and intershell rotational couplings between the various capture channels at distances R larger than at the regions of primary couplings, which will finally determine the distribution $n\ell m_{\ell}$ of the captured electron. The major difference however with the case of O^{8+}-Li($2s$) collisions is that, for Ar^{8+}-Li($2s$) collisions, the intershell rotational couplings between the capture channels correlating to nondegenerate $n\ell$ levels will be much weaker than between those correlating to degenerate or quasidegenerate levels. For these levels, the intrashell couplings will be strengthened, leading to a broadening of the m distribution; therefore, one should observe emission lines from these levels which are more depolarized than in the case of the O^{8+}-Li($2s$) collisions. These effect should be more visible for the $n=8$ capture level than for the $n=9$ capture level because the remove of the degeneracy is weaker in the latter case. This is indeed found in the CTMC calculated m distributions (see Tables II, III), and observed both in the measured and CTMC calculated polarization degrees (see Figs. 2, 3).

At very low energies, some avoided crossings between the entrance channel and the capture channels with $\ell>2$, which appear to be diabatic for the present energy range, may become efficient for radial coupling while the rotational couplings are weakened; it would result in an increase of the polarization for the emission lines of these capture sublevels. Note that in the case of the Π-electronic energies of the $(\mathrm{Ar}^{7+}+\mathrm{Li})^{+}$ system [see Fig. 4(b)], avoided crossings are also observed between the two lowest curves of the same manifold of molecular levels correlated at large distances to $n=8$ and 9 levels (respectively, at $R\approx 20$ a.u. and $R\approx 25.5$ a.u.). After transfer of the electron by radial coupling between the Σ-entrance channel and the molecular channels associated with the $8d$ and $9d$ levels, the subsequent radial coupling between the Π-molecular channels may contribute to the population of the $8p$ and $9p$ levels, and therefore may contribute to increase the population of $m=\pm 1$ sublevels with respect to the one for the O^{8+}-Li($2s$) collisions. That is observed for the CTMC calculated m distributions of the $8p$ and $9p$ levels (see Tables II, III).

It is also worth it to notice that the structure observed in the Σ-Π or Π-electronic energy curves, at distances R smaller than at the regions of primary crossings discussed above, are quite real; it is due to couplings with upper molecular states, as can be shown by diabatic calculations of the present set of electronic energies, using reduced state basis sets. Finally, we note that the regions of primary radial and rotational couplings discussed above are consistent with the maximum values of impact parameters b which contribute significantly to the CTMC calculated cross sections, that is $b_{\max}\approx 35$ a.u. for the two systems.

In conclusion, the present qualitative discussion based on the consideration of calculated electronic energy curves seem to agree on the whole with the experimental observations and the behavior of the CTMC calculated $n\ell m_{\ell}$ distributions with the energy. However, a detailed understanding of the mechanisms involved in the determination of the final $n\ell m_{\ell}$ distributions would need not only to calculate all the couplings, but also to solve the set of coupled equations for the collisional problem. This seems difficult to achieve in view of the large number of molecular channels which would be required, and because of the intricate role of the various radial and rotational couplings to be considered.

IV. CONCLUSION

We have measured the polarization degrees of lines relating to $7\ell'$-8ℓ and $8\ell'$-9ℓ transitions emitted in the near

TABLE V. Values of the parameters (in atomic units) used in the parametric potentials [Eqs. (3) and (4)] describing the electron-core interactions.

Core	Z	α_d	α_q'	r_c	A_0	A_1	A_2	B_0	B_1	B_2
Li^+	1	0.1925	−0.032	0.573	5.947	−0.849	−0.584	1.286	1.528	1.789
Ar^{8+}	8	0.3708	0.0107	0.965	63.36	34.58	−15.17	5.463	4.840	8.870

UV and the visible range by the Ar^{7+} ions produced by single-electron-capture during Ar^{8+}-Li($2s$) collisions between 1.5 keV amu^{-1} and 4.5 keV amu^{-1}. For transitions from sublevels with large ℓ values ($\ell \geq 4$), we have found a slight increase of the polarization with the collision energy, the effect vanishing as ℓ increases. CTMC calculations have shown that the projectile velocity has a small but not negligible influence on the m_ℓ-distributions, which is mainly seen for sublevels of low ℓ values. Theoretical polarization values calculated from these CTMC distributions and taking cascade effects into account are in good agreement with the experimental ones, within the error bars.

The increase of the polarization with the collision energy indicates that, after the collision, the electronic cloud tends to be more and more aligned parallel to the incident ion-beam direction. In terms of magnetic sublevel populations, it means that the probability of capture into sublevels with low m values ($m_\ell = 0, \pm 1, \pm 2$) is enhanced when the projectile velocity increases. This can be explained as due to the rotational coupling, which is more effective at high energy. At low energy, the comparison with the $(O^{7+}+Li)^+$ system allows us to assume that the projectile-core electron effect tends to depolarize the radiative emissions by promoting the intrashell broadening of the magnetic sublevel distributions.

Summarizing, the final alignment of the produced states depends in a complicated way on the behavior with the energy of the different couplings involved during the collision. But in the present work, the energy range is not large enough to induce a strong velocity effect. It would be of interest to investigate a wider energy range, more specifically at lower energies, in order to check the existence of a minimum of the polarization degree, as is supposed in Sec. III C 2. Moreover, the comparison with a projectile carrying a different core could provide more informations on the influence of the core electrons on the final states of capture. At last, for a more detailed interpretation of these m_ℓ distributions, the present work should be a basis for theoretical investigations to estimate these effects.

ACKNOWLEDGMENTS

The authors would like to thank the staff of the GANIL test bench for their efficient assistance.

APPENDIX

The electronic energies of the $(X^{7+}+Li)^+$ systems, where $X \equiv O$, Ar, are calculated by using a pseudopotential method [22–24]. For molecular structure calculations, the use of a pseudopotential is well appropriate as the core orbitals have not to be included in the state basis set expansion of the electronic wave function of the system.

In the method, the problem is reduced to a three-body interaction (the active electron and two ionic cores), where the interaction between the active electron and the two ionic cores with closed shells is described by an effective interaction. The electronic energies are then obtained by solving the one-electron Schrödinger equation

$$[H_e + \varepsilon_i(R)]\Psi_e^i = 0 \tag{A1}$$

for any distance R between the two cores (the Born-Oppenheimer approximation). As usual, the adiabatic energies $E_i(R)$ can be determined from $\varepsilon_i(R)$ by adding the interaction between the two ionic cores. The electronic Hamiltonian is defined as

$$H_e = -\tfrac{1}{2}\nabla_r + V_X + V_{\mathrm{Li}} + V_{\mathrm{CT}}, \tag{A2}$$

where V_X and V_{Li} are operators describing the effective interactions between the electron and the ionic cores. V_{CT} is a three-body interaction (the well-known cross term) which has to be included in the calculations so that the adiabatic energies $E_i(R)$ have the correct behavior at large distances. It results from the instantaneous polarization of each of the two cores by the electron and the other core [24]. In the case of O^{8+}, V_X is just the Coulomb interaction. For each core Ar^{8+} and O^{8+}, the effective interaction V_X (we will ignore the index X) is defined as

$$V = \sum_\ell V_\ell(r)\mathcal{P}_\ell - \frac{Z}{r} - \alpha_d \frac{r^2}{2(r^3+r_c^3)^2} - \alpha_q' \frac{r^3}{2(r^3+r_c^3)^4}, \tag{A3}$$

where $\mathcal{P}_\ell$ is an angular momentum projector on the core and $V_\ell(r)$ is a Gaussian-type pseudopotential

$$V_\ell(r) = A_\ell \exp(-B_\ell r^2). \tag{A4}$$

Z is the net charge of the core at large distance r. α_d is the static dipole polarizability of the core, and α_q' is an effective quadrupole polarizability including the dynamical correction to α_d. The short range semilocal pseudopotential $\Sigma_\ell V_\ell(r)\mathcal{P}_\ell$ takes into account the Pauli effects and the incomplete screening of the nucleus by the core electrons at small r distances. In practice, the summation over ℓ in Eq. (A3) can be reduced to a few values of ℓ [23]. The values of the parameters A_ℓ and B_ℓ defining $V_\ell(r)$ are determined to fit spectroscopic data of the Ar^{7+} ion and Li atom. Their values, as those of α_d, α_q' and the cutoff radius r_c are given in Table V. The electronic wave function $\Psi_e(r,R)$ is constructed using a two-center expansion in terms of a linear combination of atomic wave functions (linear combination of atomic orbitals method) for the X^{7+} ion and Li atom

$$\Psi_e(r,R) = \sum_i c_i(R)\Phi_i^X(r_X) + \sum_j d_j(R)\Phi_j^{\mathrm{Li}}(\mathbf{r}_{\mathrm{Li}}) \tag{A5}$$

Numerical wave functions are used in the expansion. They are obtained by solving the radial Schrödinger equation for the X^{7+} ion and the Li atom. For Li, the $2s$, $3s$, $2p$, $3p$, and $3d$ wave functions have been considered. For the X^{7+} ion, all the wave functions from the ground state up to the manifold of atomic states associated with the $n=15$ level have been included in the expansion. A fully numerical code has been previously developed for the molecular calculations [25], where the matrix elements are calculated by Gauss-Legendre and Gauss-Laguerre integrations. In this code, the problem of linear dependency of the state basis set expansion, which may arise when the basis set is large, is automatically controlled in the diagonalization procedure [26,27].

The electronic energies have been calculated for each symmetry Λ of the system, where Λ is the absolute value of the projection of the total orbital momentum of the system along the internuclear axis (taken as quantization axis). As a test of the numerical code, calculations have been done for the Σ electronic energies of the $(\mathrm{Ar}^{7+}+\mathrm{H})^{+}$ system for which previous one-electron diatomic molecular (OEDM) calculations [28,29] were performed. In the case of Ar^{8+}-H($1s$) collisions, the electron-capture process populates mainly the $n=5$ manifold of the Ar^{7+} ion, and all the avoided crossings between the relevant electronic energy curves calculated by our method are in good agreement with those obtained by the OEDM calculations in the range $R\sim 4-12$ a.u. Other tests of the method for the $(\mathrm{H}+\text{alkali-metal atom})^{+}$ systems have also shown good agreement with previous pseudopotential calculations using Slater-type orbitals in the atomic state expansion [23]. The present method allows us to determine the electronic energies associated with high atomic Rydberg states in the separated atom limit.

[1] R. P. Schorn, E. Hintz, D. Rusbüldt, M. Schneider, E. Unterreiter, and H. Winter, Appl. Phys. B **52**, 71 (1991).
[2] D. Dijkkamp, A. Brazuk, A. G. Drentje, F. J. de Heer, and H. Winter, J. Phys. B **17**, 4371 (1984).
[3] A. Brazuk, H. Winter, D. Dijkkamp, F. J. de Heer, and A. G. Drentje, Nucl. Instrum. Methods B **9**, 442 (1985).
[4] E. Jacquet, P. Boduch, M. Chantepie, M. Druetta, D. Hennecart, X. Husson, D. Lecler, R. E. Olson, J. Pascale, N. Stolterfoht, and M. Wilson, Phys. Scr. **47**, 618 (1993).
[5] E. Jacquet, J. Pascale, P. Boduch, M. Chantepie, and D. Lecler, Nucl. Instrum. Methods Phys. Res. Sect. B **98**, 218 (1995).
[6] E. Jacquet and J. Pascale, Nucl. Instrum. Methods Phys. Res. Sect. B **98**, 253 (1995).
[7] E. Jacquet, J. Pascale, P. Boduch, M. Chantepie, and D. Lecler, J. Phys. B **28**, 2221 (1995).
[8] J. Burgdörfer, Phys. Rev. A **24**, 1756 (1981).
[9] C. Harel and H. Jouin, J. Phys. B **21**, 859 (1988).
[10] A. Salin, J. Phys. (Paris) **45**, 671 (1984).
[11] C. Laulhé, E. Jacquet, G. Cremer, J. Pascale, P. Boduch, G. Rieger, D. Lecler, M. Chantepie, and J. L. Cojan, Phys. Rev. A **52**, 3803 (1995).
[12] D. M. Gauntt and K. Danzmann, Phys. Rev. A **46**, 5580 (1992).
[13] S. Schippers, P. Boduch, J. van Buchem, F. W. Bliek, R. Hoekstra, R. Morgenstern, and R. E. Olson, J. Phys. B **28**, 3271 (1995).
[14] U. Fano and J. F. Macek, Rev. Mod. Phys. **45**, 553 (1973).
[15] R. Abrines and I. C. Percival, Proc. Phys. Soc. **88**, 861 (1966).
[16] R. E. Olson and A. Salop, Phys. Rev. A **16**, 531 (1977).
[17] J. Pascale, R. E. Olson, and C. O. Reinhold, Phys. Rev. A **42**, 5305 (1990).
[18] R. E. Olson, J. Pascale, and R. Hoekstra, J. Phys. B **25**, 4241 (1992).
[19] C. E. Theodosiou, M. Inokuti, and S. T. Manson, At. Data Nucl. Data Tables **19**, 473 (1986).
[20] C. D. Lin and J. H. Macek, Phys. Rev. A **35**, 5005 (1987).
[21] L. J. Lembo, K. Danzmann, Ch. Stoller, W. E. Meyerhof, and T. W. Hänsch, Phys. Rev. A **37**, 1141 (1988).
[22] J. N. Bardsley, Case Stud. At. Phys. **4**, 299 (1974).
[23] M. Kimura, R. E. Olson, and J. Pascale, Phys. Rev. A **26**, 3113 (1982).
[24] J. Pascale, Phys. Rev. A **26**, R3709 (1982).
[25] J. Pascale (unpublished).
[26] J. C. Nash, Comput. Phys. Commun. **8**, 85 (1974).
[27] P. Valiron, 3rd cycle thesis *n*° **1279**, Univ. Bordeaux I (1976).
[28] H. Jouin, thesis *n*° **94**, Univ. Bordeaux I (1986).
[29] C. Harel and H. Jouin, J. Phys. B **21**, 859 (1988).